

LETTER • OPEN ACCESS

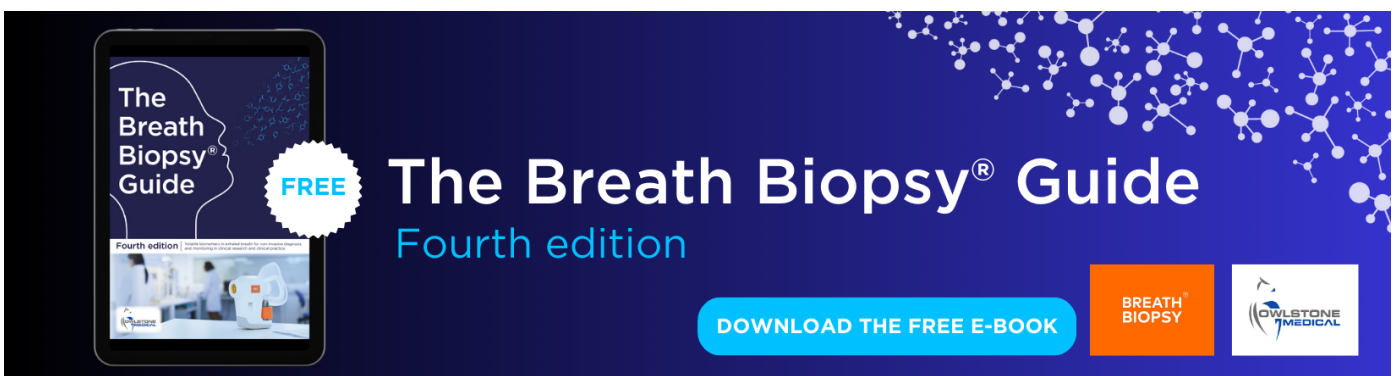
The impact of stratospheric aerosol heating on the frozen hydrometeor transport pathways in the tropical tropopause layer

To cite this article: C A Kroll *et al* 2024 *Environ. Res. Lett.* **19** 044039

View the [article online](#) for updates and enhancements.

You may also like

- [Linking global land surface temperature projections to radiative effects of hydrometeors under a global warming scenario](#)
J-L F Li, Kuan-Man Xu, Wei-Liang Lee et al.
- [Experimental investigation on streamer inception from artificial hydrometeors](#)
S Mirpour and S Nijdam
- [Outlook research of application of model hydrometeor arrays for artificial initiation of lightning and thundercloud charge reduction](#)
A G Temnikov, D S Zhuravkova, A V Orlov et al.



The Breath Biopsy® Guide
Fourth edition

FREE

DOWNLOAD THE FREE E-BOOK

BREATH BIOPSY

OWLSTONE MEDICAL

ENVIRONMENTAL RESEARCH
LETTERS

LETTER

OPEN ACCESS

RECEIVED
1 December 2023REVISED
30 January 2024ACCEPTED FOR PUBLICATION
14 March 2024PUBLISHED
26 March 2024

Original Content from
this work may be used
under the terms of the
[Creative Commons
Attribution 4.0 licence](#).

Any further distribution
of this work must
maintain attribution to
the author(s) and the title
of the work, journal
citation and DOI.

The impact of stratospheric aerosol heating on the frozen
hydrometeor transport pathways in the tropical tropopause layerC A Kroll^{1,2,*} , S Fueglistaler³, H Schmidt¹, T Dauhut⁴ and C Timmreck¹ ¹ Max Planck Institute for Meteorology, Hamburg, Germany² Institute for Atmospheric and Climate Science, ETH Zurich, Zurich, Switzerland³ Program in Atmospheric and Oceanic Sciences, Princeton University, Princeton, NJ, United States of America⁴ LAERO, Université de Toulouse, CNRS, UT3, IRD, Toulouse, France

* Author to whom any correspondence should be addressed.

E-mail: clarissa.kroll@env.ethz.ch**Keywords:** stratospheric moisture budget, deep convection, heating perturbation, tropical tropopause layer, volcano, geoengineering**Abstract**

The exceptionally low temperature in the tropical tropopause layer (TTL) restricts the amount of water vapor entering the stratosphere. However, moisture may also enter the stratosphere in its frozen state, and the amount thereof depends on hydrometeor sedimentation and air vertical velocity. We investigate the sensitivity of frozen hydrometeor transport pathways to substantial perturbations of the TTL temperature structure in global storm-resolving model simulations. A special focus is laid on the question which process—convection, slow upwelling within the background velocity field, in-cloud radiative processes, gravity waves or turbulence—is responsible for most of the transport. The study shows that the main contribution to the frozen hydrometeor flux is cold-point overshooting convection in both the control and perturbed scenario. The average convective event transports an increased amount of frozen hydrometeors at the cold-point tropopause, when the later is warmed. This finding can be explained by scaling of frozen moisture content with Clausius Clapeyron in a saturated environment.

1. Introduction

Stratospheric water vapor is known as an important greenhouse gas [1] and vital player in stratospheric chemistry [2]. The very low temperatures in the tropical tropopause layer (TTL [3]) constrain the water entering the stratosphere to no more than a few parts per million [4], and seasonal and interannual variability in water entering the stratosphere is also well explained by variations in tropical tropopause temperatures [5–7]. However, the partitioning of water entering the stratosphere between vapor and frozen hydrometeors, and between the different processes contributing to the frozen hydrometeor flux, remain insufficiently quantified. Especially, the reliability of frozen moisture budgets obtained with general circulation model simulations is uncertain as they heavily rely on parameterized convection [8–11].

The advent of global storm-resolving models (GSRM, [12–14]) allows to investigate the importance of individual frozen hydrometeor pathways within a single, coherent model explicitly resolving

many of the dynamical processes involved such as deep convection [15, 16], dynamically forced slow upwelling [4], cloud lofting from cloud radiative heating [17] as well as in-cloud turbulence and gravity waves [18, 19]. GSRMs are also able to simulate both the large-scale mean flow and dynamically forced slow ascent [20], which can not be captured by limited-domain models. This makes GSRMs an ideal tool to study the moisture budgets in the TTL as they capture both the large-scale state and the convection scale and yield a realistic representation of deep convection [21, 22]. Here, we present the results from GSRM simulations with the Icosahedral Nonhydrostatic Weather and Climate Model, ICON, using a horizontal resolution of 10 km and a vertical resolution of 500 m in the TTL. We analyse the spectrum of cross-tropopause frozen hydrometeor fluxes as function of vertical velocity in a control simulation (CTL), and a simulation with strongly perturbed temperatures in the TTL (PTB). These simulations show a remarkable insensitivity of the flux partitioning in vapor and frozen phase to the

TTL temperature perturbation [23], raising the question why the frozen hydrometeor flux scales—like the vapor flux—to good approximation with the Clausius–Clapeyron rate.

Different processes are thought to be of importance for frozen hydrometeor transport into the stratosphere. Specifically, the processes of interest include tropopause-penetrating deep convection, in-cloud turbulence and gravity waves. Furthermore we consider that thin cirrus clouds may be lofted into the stratosphere by the dynamically forced mean-upwelling of the (shallow) Brewer–Dobson circulation, or that differential radiative heating between a cloud and its surrounding may actively lead to a lofting of the cloud. The named processes differ in the characteristics of their vertical velocities. Corti *et al* [17] estimate average in-cloud heating velocities to be of order mm s^{-1} , similar to the mean upwelling [3, 24]. The magnitude of gravity waves and in-cloud turbulence is much larger (order m s^{-1}), but may lead to compensating up- and downward movement [18, 19], whereas overshooting deep convection occurs at velocities up to the order m s^{-1} . We chose to use the vertical wind field to distinguish between the different transport pathways rather than using a classification based on feature-detection which may produce results biased by the feature criteria and difficult to reproduce by others. Thus, the analysis is objective, but the association with specific processes is only semi-quantitative. In the following, we first describe the model and simulations, as well as the method to quantify the cross-tropopause frozen hydrometeor flux. We then discuss the results, and interpretation thereof in the context of the above processes, and conclude with conclusions and outlook.

2. Methods

2.1. Model simulations

2.1.1. Model setup

This study analyzes the storm-resolving simulations described in [23]. The simulations are performed with the atmosphere component of the Icosahedral Nonhydrostatic Weather and Climate Model (ICON-A, [22, 25, 26]). The horizontal grid spacing is 10 km. In the vertical, 90 layers are simulated up to a model top at 75 km. This yields a vertical resolution of 500 m–700 m in the TTL, identical to the setting used in the DYAMOND simulations [12]. Boundary conditions for ozone and sea surface temperatures for January 2020 are prescribed.

In the GSRM, gravity waves and convection are explicitly calculated without the use of parametrizations [22]. This procedure has rendered superior results at same resolution compared to simulations relying on convective parametrizations [11]. Radiative transfer is calculated with the PSrad radiation parametrization [27]. Microphysical processes

are simulated with a one-moment microphysics scheme (an update version of Baldauf *et al* [28]), which represents six water categories water vapor, cloud water, cloud ice, rain, graupel and snow.

2.1.2. Experiments

We analyze two experiments: an unperturbed control run (CTL) and a perturbed run (PTB) with an additional heating source in the TTL and lower stratosphere.

The diabatic heating perturbation in PTB is implemented with radiative heating from a height-latitude dependent sulfate aerosol layer as may be used to study the effects of volcanic eruptions and aerosol geoengineering. The aerosol is described by its optical properties—single scattering albedo, extinction and asymmetry factor—in 16 terrestrial and 14 solar bands. The corresponding input files are generated offline with the easy volcanic aerosol forcing generator [29]. The initially emitted sulfur amounts to 20 Tg S which corresponds approximately to twice the sulfur emission of the Mt. Pinatubo eruption (i.e. [30]). Within the simulation the volcanic aerosol forcing distribution is set constant to the month of highest IR extinction. The heating perturbation is deliberately chosen to lead to a strong temperature change in the TTL and correspondingly a robust signal in the changes in the cross-tropopause fluxes.

Both simulations run with identical boundary conditions fixed to 1 January 2020 to exclude seasonal effects from the analysis. The spin-up time for the simulations consists of 150 model days allowing the temperature profiles to adjust to the aerosol forcing. The following analysis is based on the subsequent two perpetual January months.

2.2. Budget calculations

We perform a moisture budget calculation to determine the convective influence on the moisture fluxes at the tropical cold-point tropopause. For this purpose the individual terms of the continuity equation, which describes the temporal change in specific moisture q_i with $i \in \{\text{water vapor, cloud water, rain, cloud ice, graupel, snow}\}$, are analyzed:

$$\frac{\partial \rho q_i}{\partial t} = - \underbrace{\left(\frac{\partial \rho q_i u}{\partial x} + \frac{\partial \rho q_i v}{\partial y} + \frac{\partial \rho q_i w}{\partial z} \right)}_{\text{advection and grid-scale turbulence}} - \underbrace{\left(\frac{\partial \rho q_i w_{\text{sed},i}}{\partial z} \right)}_{\text{sedimentation}} + \underbrace{\nabla \cdot (D \nabla \rho q_i)}_{\text{subgrid-scale turbulence}} + \underbrace{\sigma_i}_{\text{microphysical conversion processes}}, \quad (1)$$

where u, v, w are the velocities of the background field, $w_{\text{sed},i}$ is the sedimentation velocity, ρ the atmospheric density, D describes the subgrid-scale turbulent diffusion, and σ_i accounts for the sources and sinks of q_i due to microphysical processes. The vertical advection (which includes resolved turbulence), the

sedimentation, subgrid-scale turbulent diffusion and microphysical conversion processes are output directly from the model.

In the following we analyze the corresponding vertical moisture transport at the $[-30, 30]^\circ\text{N}$ and time averaged cold-point tropopause (compare Fueglistaler *et al* [3]) for the two months of perpetual January simulations of both experiments. The cold-point tropopause height is defined here as the height with lowest temperature between the troposphere and stratosphere on model levels of the native grid.

2.3. Analysis of cold-point overshooting convection

A convective event which injects frozen hydrometeors above the local instantaneous cold-point tropopause is considered a cold-point overshoot [31]. In order to prevent misattribution of convective events as cold-point overshoots we chose a very strict measure for cold-point overshoots: convective events with a level of neutral buoyancy (LNB) above the local cold-point tropopause. The LNB is estimated for convective updrafts with the potential to overshoot the cold-point tropopause. These convective updrafts are selected based on a threshold vertical velocity of 3 and 5 m s^{-1} at a height of 10 km. A recursive algorithm identifies the entire convective updrafts and a contiguous, three grid cell wide surrounding. Then the average temperature profiles of convective updrafts and their surroundings are compared. The lowest height at which the temperature of the surrounding exceeds the temperature of the convective updrafts is the estimate of the current LNB. The cold-point overshoot analysis is performed in a sub-area between $[0, 10]^\circ\text{N}$, which contains the majority of deep convective events in the tropics during the analyzed month of January.

3. Results

3.1. Characterization of the cold-point tropopause perturbation

figure 1 shows the average temperature profiles of CTL (blue) and PTB (red) in the tropics from $[-30, 30]^\circ\text{N}$. The applied heating perturbation, represented by a dotted black line, leads to a warming from about 14 km altitude upwards. In consequence the cold-point tropopause shifts downwards from 17.5 km in CTL to 16.4 km in PTB and is 9.2 K warmer in PTB than in CTL.

3.2. Overshooting convection as dominant transport pathway for (increased) frozen hydrometeors

The analysis of these simulations by Kroll *et al* [23] showed that both water vapor and total frozen hydrometeor fluxes at the cold-point tropopause are enhanced, while conserving a 80:20 partitioning ratio between vapor and frozen moisture flux (cf table 1).

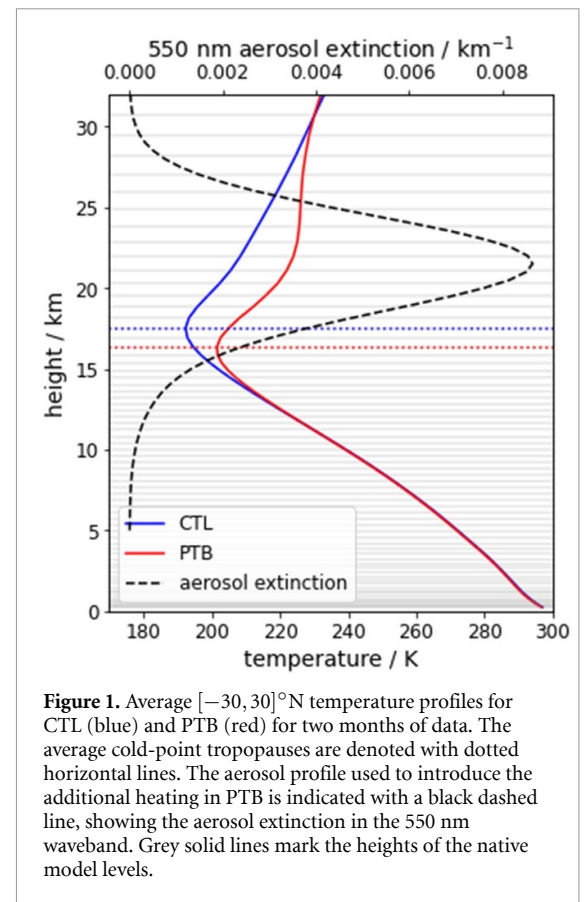


Figure 1. Average $[-30, 30]^\circ\text{N}$ temperature profiles for CTL (blue) and PTB (red) for two months of data. The average cold-point tropopauses are denoted with dotted horizontal lines. The aerosol profile used to introduce the additional heating in PTB is indicated with a black dashed line, showing the aerosol extinction in the 550 nm waveband. Grey solid lines mark the heights of the native model levels.

In CTL and PTB, the largest share of frozen hydrometeor originates from cloud ice, followed by graupel and snow.

Processes responsible for the frozen hydrometeor transport can be either fast cold-point overshooting convection or slower transport such as the dynamical slow upwelling, radiatively induced upwelling, turbulence or gravity wave effects. In the following we investigate which is the dominant transport pathway and if the relative importance between different pathways changes between CTL and PTB.

The subgrid-scale turbulent diffusion is directly computed from the budget equation, as it corresponds to one of the tendency terms in the budget equation and is directly output from the model. In the model, turbulent diffusion is only applied to water vapor and the lightest frozen hydrometeor, cloud ice. Vertical gradients of ice content are steeper than those of water vapor as cloud ice is not as homogeneously distributed as water vapor. This explains the stronger turbulent frozen hydrometeor flux compared to the vapor moisture flux in CTL. In PTB, both turbulent mixing terms are enhanced compared to CTL, which can be linked to generally even steeper moisture gradients in the TTL arising from the higher TTL temperatures in PTB. However, the turbulent contribution to the frozen cloud ice flux is an order of magnitude smaller than the advective and sedimentation contributions in both scenarios (cf table 1).

Table 1. Moisture fluxes through the time- and spatially-averaged tropical cold-point tropopause for CTL and PTB in the area between $[-30, 30]^\circ\text{N}$. The contribution of advective and sedimentation fluxes as well as subgrid-scale turbulent diffusion are listed. Turbulent diffusion is only applied to water vapor and cloud ice.

Flux/g m ⁻² year ⁻¹	Advection & sedimentation		Turbulent diffusion (subgrid-scale)		Total	
	CTL	PTB	CTL	PTB	CTL	PTB
water vapor	2.095	8.097	0.004	0.020	2.099	8.116
cloud ice	0.375	1.200	0.029	0.190	0.404	1.392
snow	0.092	0.304	—	—	0.092	0.304
graupel	0.121	0.559	—	—	0.121	0.559

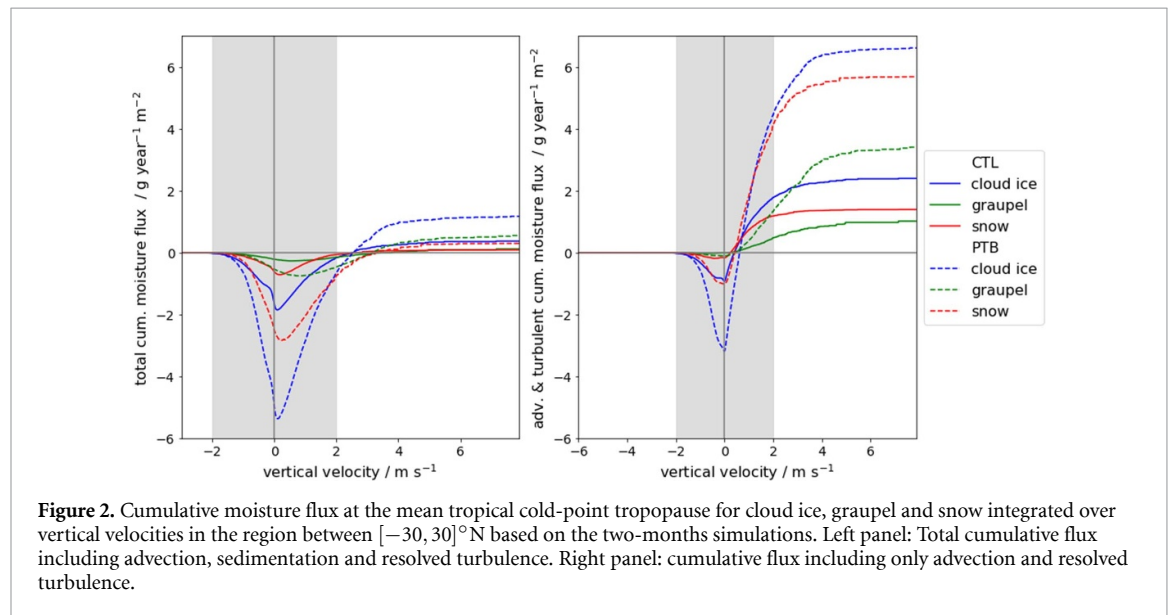


Figure 2. Cumulative moisture flux at the mean tropical cold-point tropopause for cloud ice, graupel and snow integrated over vertical velocities in the region between $[-30, 30]^\circ\text{N}$ based on the two-months simulations. Left panel: Total cumulative flux including advection, sedimentation and resolved turbulence. Right panel: cumulative flux including only advection and resolved turbulence.

Consequently, the major flux contribution originates from the remaining slow non-convective processes or faster processes of cold-point overshooting convection. A first discrimination between the remaining moisture transport paths is possible based on their velocities. We therefore analyse the cumulative advection, grid-scale turbulence and sedimentation moisture flux integrated over the vertical velocities at the cold-point tropopause (see figure 2(a)) based on the two months of simulations. The figure shows the individual hydrometeors fluxes. Slow upwelling within the background velocity field, in-cloud upwelling, turbulence and gravity waves have typical vertical velocity range of $[-2, 2] \text{ m s}^{-1}$ [3, 18, 19, 24], indicated by the grey shading. The cumulative moisture flux shown in figure 2(a) only shows a net positive transport at positive velocities outside the $[-2, 2] \text{ m s}^{-1}$. The net positive frozen moisture transport in the higher velocity ranges shows that overshooting convection is responsible for the majority of the net frozen moisture transport. This is true both for CTL and PTB. The perturbation does not lead to a substantial redistribution of the percental share of frozen moisture transported in individual velocity ranges but rather increases the absolute amount of frozen moisture in each velocity range transported in the PTB scenario.

In the $[-2, 2] \text{ m s}^{-1}$ region various processes can occur ranging from slow upwelling, in-cloud turbulence, gravity waves, ceasing convection and in-cloud upwelling. The cumulative flux is almost symmetric around zero vertical velocity in the $[-2, 2] \text{ m s}^{-1}$ velocity range for the lighter hydrometeors cloud ice and snow. This is an indication of a turbulence controlled regime or a height-stabilized layer of ultra thin clouds [32, 33]. To investigate the role of sedimentation for the net flux we show the cumulative flux attributable to advection and grid-scale turbulence in figure 2(b). Here it becomes evident that neglecting the sedimentation velocities in the low velocity range would give the impression that most moisture is transported by turbulence, ceasing convection, slow ascent and in-cloud upwelling. As the advective flux is not purely symmetric around zero—as would be expected for pure turbulence—but has a steep slope at positive velocities, it can be assumed that this velocity range is not purely turbulence dominated.

3.3. Increased mass transport per convective event

Two possibilities exist for the increased frozen hydrometeor flux via cold-point overshooting convection found in section 3.2: an increased frequency of cold-point overshooting events and/or an increased mass transport per convective event. In order to determine

Table 2. Summary of the analysis of overshoots above the local instantaneous cold-point tropopause: Investigations for convective events exceeding a the 3 m s^{-1} and 5 m s^{-1} vertical velocity thresholds at 10 km. Total number of analyzed events fulfilling the selection criteria, number of potential cold-point tropopause overshoots within this group, and percentage of potential cold-point tropopause overshoots for CTL and PTB selected over two months in perpetual January mode.

	total events		overshoots		overshoot percentages	
	3 m s^{-1}	5 m s^{-1}	3 m s^{-1}	5 m s^{-1}	3 m s^{-1}	5 m s^{-1}
CTL	310 943	86 713	1984	818	0.64	0.94%
PTB	268 287	71 769	2707	862	1.01	1.2%

the dominant feature we first analyze the frequency of convective events based on the calculation of instantaneous LNBS (cf section 2.3). Table 2 summarizes the corresponding statistics for velocity thresholds of 3 m s^{-1} and 5 m s^{-1} . In PTB a decrease in the frequency of high velocity convective updrafts at 10 km is denoted with -13% for the 3 m s^{-1} and -18% for the 5 m s^{-1} threshold, which also indicates a reduction in the vigorousness of convective events. This matches expectations, as the stability in the TTL is increased and the sub-cloud moist static energy is decreased due to aerosol induced land surface temperature reductions. Nevertheless, the number of overshoots above the local instantaneous cold-point tropopause stays approximately constant or only increases slightly in PTB both in absolute and relative numbers. The increase in percentage share of overshooting events amounts to around $+0.4\%$ when normalized to the total number of convective events analyzed, whereas the number of overshoots is enhanced by a factor of 1.36 for the 3 m s^{-1} and 1.05 for the 5 m s^{-1} threshold. The total number of overshoots thus increases by $+36\%$ at most, whereas the frozen hydrometeor flux increases by $+300\%$ – 400% . This potential small increase of overshooting events can not explain the magnitude of the flux increase.

We therefore analyze the total transported frozen hydrometeor content normalized by the number of (convective) events. Figure 3 shows the specific hydrometeor content at the cold-point tropopause binned according to percentiles of column integrated water vapor. Although the specific frozen hydrometeor content in PTB is increased throughout the entire tropical cold-point tropopause, the absolute increase is dominated by the increase in the highest percentiles corresponding to deep convective activity (e.g. Schulz and Stevens [34]). As the values are normalized to the number of analyzed events, the higher values in PTB compared to CTL demonstrate that more frozen hydrometeor mass is transported within the average convective event. Indeed, the corresponding increase in frozen hydrometeor mass transported per convective event increases by $+300\%$ in the highest percentiles, nicely matching the flux increase.

The increase in transported frozen mass can be explained by the higher temperatures around the cold-point tropopause in PTB: According to the Clausius Clapeyron scaling of saturation specific

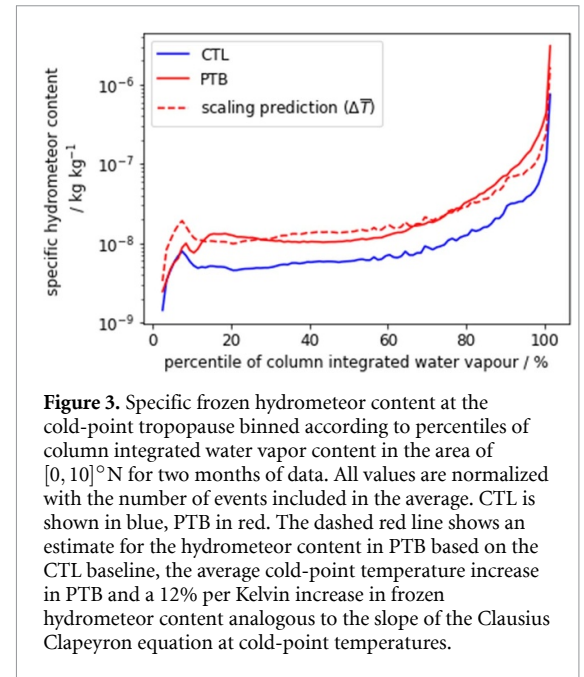


Figure 3. Specific frozen hydrometeor content at the cold-point tropopause binned according to percentiles of column integrated water vapor content in the area of $[0, 10]^\circ\text{N}$ for two months of data. All values are normalized with the number of events included in the average. CTL is shown in blue, PTB in red. The dashed red line shows an estimate for the hydrometeor content in PTB based on the CTL baseline, the average cold-point temperature increase in PTB and a 12% per Kelvin increase in frozen hydrometeor content analogous to the slope of the Clausius Clapeyron equation at cold-point temperatures.

humidity with temperature, every Kelvin decrease in temperature when approaching the cold-point tropopause will lead to 10% vapor freezing out in saturated air parcels at the cold-point tropopause. At elevated temperatures the air can carry more water vapor. Correspondingly, the freeze-out of 10% of the total water vapor at saturation will give a larger absolute amount of frozen hydrometeors generated per Kelvin temperature decrease. The enhanced cross-tropopause flux of frozen hydrometeors can therefore be explained by a Clausius–Clapeyron scaling of frozen hydrometeor content, while changes in the frequency of cold-point overshooting convection play no significant role.

We test this by estimating the PTB specific frozen hydrometeor content using Clausius Clapeyron scaling. The dashed red line shows the estimate of the frozen hydrometeor content when only considering the Clausius Clapeyron scaling. It is calculated based on the average cold-point temperature increases in the corresponding bins and assumes a 12% per Kelvin increase in frozen hydrometeor content with the frozen hydrometeor content in CTL as baseline. Although solely based on average temperatures instead of the lowest inner-tropical temperatures, which are mainly responsible for the

freeze-drying (e.g. Oman *et al* [35]), it can be used as a estimate of the frozen hydrometeor content in PTB. Only in the highest percentiles of column integrated water vapor, the most convective regions, this approximation becomes less accurate, e.g. underestimate the frozen moisture amount. This could be partly caused by the vertical velocities of much higher absolute magnitude than the sedimentation velocities (e.g. less fallout), less exposure to the temperature variability in the higher atmospheric layers within the fast ascent of convective cores, and increased ice formation rates within the convective cores.

4. Discussion and conclusion

We investigated the sensitivity of frozen hydrometeor transport pathways to external forcing in the tropical cold-point tropopause using the GSRM version of ICON. The analysis shows that cold-point overshooting convection is the most important transport pathway for frozen hydrometeors in the tropical cold-point tropopause, both in PTB and CTL. The prominence of convective events in the tropical cold-point tropopause is in line with the findings by a model- and an observation-based study [36, 16].

The model calculations analyzed here do not find support for net transport by cloud lifting due to in-cloud radiative heating proposed by Corti *et al* [17]. However, the investigation reveals that, when not considering the sedimentation velocities (cf figure 2(b)), a large fraction of frozen moisture is advected in the velocity range containing the in-cloud upwelling transport pathway. Corti *et al* only investigated the pure radiative heating derived mass fluxes, which may explain the dominance of in-cloud upwelling in their analysis.

Cirrus clouds formation can also be induced by gravity waves in the tropical cold-point tropopause (i.e. [19, 37]). Our analysis indicates that the frozen hydrometeors formed by gravity wave induced events do not contribute considerably to the net transport as the associated upward transport is counterbalanced by downward transport (cf figure 2). This finding is in agreement with Podglajen *et al* [18] who find that ice clouds affected by gravity waves only show a decreased downward propagation speed but no net upward movement.

In the tropical cold-point tropopause the diffusivity decreases rapidly with height (i.e. [38, 39]) resulting in a decrease of the moisture flux due to sub-grid turbulent mixing compared to the lower troposphere, making it the smallest flux contributor in our simulations. Although these results make physical sense, we want to point out that turbulent mixing is still ill constrained in numerical models. Obtaining high quality observational constraints for turbulent mixing at the tropical cold-point tropopause, in clear sky and even more importantly cloudy sky, would be an

invaluable contribution to improve upon one of the last few remaining parametrizations in GSRMs.

In the heating perturbation experiment, the frozen hydrometeor fluxes corresponding to all three pathways are enhanced, with cold-point overshooting convection remaining the predominant transport pathway. The increase in frozen hydrometeor flux within convective events simulated for a tropical cold-point tropopause temperature increase may seem contradictory to the reduction of upper tropospheric clouds found in other studies (i.e. [40–42]). Both findings can however be reconciled by considering the frozen hydrometeor distribution with respect to the cold-point tropopause height. Our simulations also show a decrease in the absolute frozen hydrometeor content at the height of main convective outflow. The situation however changes as we approach the TTL and the increase in TTL temperatures in perturbed scenario becomes more prominent. As the air is near saturation in the TTL the higher temperatures will translate into a higher absolute vapor content. Correspondingly the potential for frozen hydrometeor creation as air parcels rise and their temperature decreases is enhanced in the heating perturbation experiment. This can be seen when considering the slope of the Clausius Clapeyron equation which would dictate a decrease of around 10% of water vapor per Kelvin decrease in temperature [43] in the TTL—a scaling which is reflected in the frozen mass content of convective towers. The increase in frozen hydrometeor content in the height levels near the cold-point tropopause will not be captured when regarding only zonal differences of height dependent moisture distribution as the cold-point tropopause is shifted downwards in the perturbed scenario.

The exact numerical results may be model specific and subject to the choice of microphysical and turbulence parametrizations (e.g. [38, 44]). In our study, we focused on the effect of a large temperature perturbation in the TTL on water transport into the stratosphere. Such a strong temperature perturbation may arise from the radiative heating of a large perturbation of stratospheric aerosol, or any other event or process that significantly affects the TTL heat budget. In the aerosol scenario, the aerosol perturbation may also impact cloud microphysical processes in the TTL, which in turn may also have an impact on the amount of moisture entering the stratosphere. Presently, model simulations as used here remain computationally extremely expensive, and in this pioneering study the model's cloud microphysics had to be run without information about the increased aerosol burden. Our study may provide additional motivation to complement the high horizontal resolution of GSRMs with cloud microphysical schemes that allow to study aerosol-cloud microphysical interactions.

In summary we showed that

- (i) frozen hydrometeors are predominantly transported within cold-point overshooting convective events in the tropical tropopause layer.
- (ii) under heating perturbations in the tropical tropopause layer and lower stratosphere
 - the frequency of cold-point overshooting convection remains unchanged.
 - the average cold-point overshooting event transports an increased amount of frozen hydrometeors.

The results of this study highlight the importance of changes in the large-scale TTL temperature field for the total mass in frozen hydrometeor transported in convective events. They are in agreement with other studies on the vapor-frozen hydrometeor partitioning under other perturbations like seasonal variations [45, 46] or climate change [47]. The increase in tropical cold-point tropopause temperatures leads to an increased absolute amount of water vapor within saturated air parcels which can freeze out. Following the 10% water vapor freezing out per Kelvin decrease in temperature at saturation, frozen hydrometeor production is enhanced and more frozen hydrometeors are transported within convective cores at the height of the cold-point tropopause.

Data availability statement

This work analyses the simulations described in [23]. Further analysis scripts needed to reproduce the work presented in this paper are stored under <https://hdl.handle.net/21.11116/0000-000D-F723-5>.

Acknowledgments

This research has been supported by the Deutsche Forschungsgemeinschaft (DFG) Research Unit VollImpact (FOR2820, Grant No. 398006378) within the projects VolDyn and VolClim. The data was processed using CDO (<https://code.mpimet.mpg.de/projects/cdo/embedded/cdo.pdf>) and the resources at the Deutsche Klimarechenzentrum (DKRZ) granted by its Scientific Steering Committee (WLA) under Project ID bb1093. For parts of the analysis the open source library ‘netcdf’ by J Colvin (<https://code.dlang.org/packages/netcdf>) were employed. We thank J Radtke, A Schneidereit, U Niemeier, J Bao, B Goger, L Kornblueh as well as L Kluft for discussing different aspects of this work with the authors.

Conflict of interest

The authors have no conflict of interest to declare.

ORCID iDs

C A Kroll  <https://orcid.org/0000-0002-3449-418X>

C Timmreck  <https://orcid.org/0000-0001-5355-0426>

References

- [1] Solomon S, Rosenlof K H, Portmann R W, Daniel J S, Davis S M, Sanford T J and Plattner G-K 2010 Contributions of stratospheric water vapor to decadal changes in the rate of global warming *Science* **327** 1219–23
- [2] Ko M K W, Newman P A, Reimann S, and Strahan S E 2013 SPARC report on lifetimes of stratospheric ozone-depleting substances, their replacements, and related species *Technical Report* SPARC Office
- [3] Fueglistaler S, Dessler A E, Dunkerton T J, Folkins I, Fu Q and Mote P W 2009 Tropical tropopause layer *Rev. Geophys.* **47** 1606
- [4] Brewer A W 1949 Evidence for a world circulation provided by the measurements of helium and water vapour distribution in the stratosphere *Q. J. R. Meteorol. Soc.* **75** 351–63
- [5] Mote P W, Rosenlof K H, McIntyre M E, Carr E S, Gille J C, Holton J R, Kinnerson J S, Pumphrey H C, Russell J M and Waters J W 1996 An atmospheric tape recorder: the imprint of tropical tropopause temperatures on stratospheric water vapor *J. Geophys. Res.: Atmos.* **101** 989–4006
- [6] Fueglistaler S, Bonazzola M, Haynes P H and Peter T 2005 Stratospheric water vapor predicted from the Lagrangian temperature history of air entering the stratosphere in the tropics *J. Geophys. Res.: Atmos.* **110** D08107
- [7] Randel W J, Wu F, Vömel H, Nedoluha G E and Forster P 2006 Decreases in stratospheric water vapor after 2001: links to changes in the tropical tropopause and the Brewer-Dobson circulation *J. Geophys. Res.: Atmos.* **111** D12312
- [8] Arakawa A 2004 The cumulus parameterization problem: past, present and future *J. Clim.* **17** 2493–525
- [9] Jones T R and Randall D A 2011 Quantifying the limits of convective parameterizations *J. Geophys. Res.: Atmos.* **116** D08210
- [10] Sherwood S C, Bony S and Dufresne J-L 2014 Spread in model climate sensitivity traced to atmospheric convective mixing *Nature* **505** 37–42
- [11] Vergara-Temprado J, Ban N, Panosetti D, Schlemmer L and Schär C 2020 Climate models permit convection at much coarser resolutions than previously considered *J. Clim.* **33** 1915–33
- [12] Stevens B et al 2019 DYAMOND: the dynamics of the atmospheric general circulation modeled on non-hydrostatic domains *Prog. Earth Planet. Sci.* **6** 61
- [13] Satoh M, Stevens B, Judt F, Khairoutdinov M, Lin S-J, Putman W M and Dübén P 2019 Global cloud-resolving models *Curr. Clim. Change Rep.* **5** 172–84
- [14] Hohenegger C, Kornblueh L, Klocke D, Becker T, Cioni G, Frederik Engels J, Schulzweida U and Stevens B 2020 Climate statistics in global simulations of the atmosphere, from 80 to 2.5 km grid spacing *J. Meteorol. Soc. Japan Ser. II* **98** 73–91
- [15] Dauhut T, Chaboureau J-P, Haynes P H and Lane T P 2018 The mechanisms leading to a stratospheric hydration by overshooting convection *J. Atmos. Sci.* **75** 4383–98

- [16] Bolot M and Fueglistaler S 2021 Tropical water fluxes dominated by deep convection up to near tropopause levels *Geophys. Res. Lett.* **48** e2020GL091471
- [17] Corti T, Luo B, Fu Q, Vömel H and Peter T 2006 The impact of cirrus clouds on tropical troposphere-to-stratosphere transport *Atmos. Chem. Phys.* **6** 2539–47
- [18] Podglajen A, Plougonven R, Hertzog A and Jensen E 2018 Impact of gravity waves on the motion and distribution of atmospheric ice particles *Atmos. Chem. Phys.* **18** 10799–823
- [19] Atlas R and Bretherton C S 2022 Aircraft observations of gravity wave activity and turbulence in the tropical tropopause layer: prevalence, influence on cirrus and comparison with global-storm resolving models *Atmos. Chem. Phys. Discuss.* **2022** 1–30
- [20] Haynes P H, McIntyre M E, Shepherd T G, Marks C J and Shine K P 1991 On the ‘downward control’ of extratropical diabatic circulations by Eddy-induced mean zonal forces *J. Atmos. Sci.* **48** 651–78
- [21] Dauhut T and Hohenegger C 2022 The contribution of convection to the stratospheric water vapor: the first budget using a global storm-resolving model *J. Geophys. Res.: Atmos.* **127** e2021JD036295
- [22] Hohenegger C et al 2022 ICON-sapphire: simulating the components of the earth system and their interactions at kilometer and subkilometer scales *Geosci. Model Dev. Discuss.* **16** 1–42
- [23] Kroll C A, Fueglistaler S, Schmidt H, Kornblueh L and Timmreck C 2023 The sensitivity of moisture flux partitioning in the cold-point tropopause to external forcing *Geophys. Res. Lett.* **50** e2022GL102262
- [24] Plumb R A 2002 Stratospheric transport *J. Meteorol. Soc. Japan Ser. II* **80** 793–809
- [25] Crueger T et al 2018 The atmosphere component of the ICON earth system model: II. Model evaluation *J. Adv. Model. Earth Syst.* **10** 1638–62
- [26] Giorgetta M A et al 2018 ICON-a, the atmosphere component of the ICON earth system model: I. Model description *J. Adv. Model. Earth Syst.* **10** 1613–37
- [27] Pincus R and Stevens B 2013 Paths to accuracy for radiation parameterizations in atmospheric models *J. Adv. Model. Earth Syst.* **5** 225–33
- [28] Baldauf M, Seifert A, Förstner J, Majewski D, Raschendorfer M and Reinhardt T 2011 Operational convective-scale numerical weather prediction with the COSMO model: description and sensitivities *Mon. Weather Rev.* **139** 3887–905
- [29] Toohey M, Stevens B, Schmidt H and Timmreck C 2016 Easy volcanic aerosol (EVA v1.0): an idealized forcing generator for climate simulations *Geosci. Model Dev.* **9** 4049–70
- [30] Timmreck C et al 2018 The interactive stratospheric aerosol model intercomparison project (ISA-MIP): motivation and experimental design *Geosci. Model Dev.* **11** 2581–608
- [31] Danielsen E F 1993 *In situ* evidence of rapid, vertical, irreversible transport of lower tropospheric air into the lower tropical stratosphere by convective cloud turrets and by larger-scale upwelling in tropical cyclones *J. Geophys. Res.* **98** 8665–81
- [32] Peter T et al 2003 Ultrathin tropical tropopause clouds (UTTCs): I. Cloud morphology and occurrence *Atmos. Chem. Phys.* **3** 1083–91
- [33] Luo B P et al 2003 Ultrathin tropical tropopause clouds (UTTCs): II. Stabilization mechanisms *Atmos. Chem. Phys.* **3** 1093–100
- [34] Schulz H and Stevens B 2018 Observing the tropical atmosphere in moisture space *J. Atmos. Sci.* **75** 3313–30
- [35] Oman L, Waugh D W, Pawson S, Stolarski R S and Eric Nielsen J 2008 Understanding the changes of stratospheric water vapor in coupled chemistry climate model simulations *J. Atmos. Sci.* **65** 3278–91
- [36] Nugent J M, Turbeville S M, Bretherton C S, Blossey P N and Ackerman T P 2022 Tropical cirrus in global storm-resolving models: 1. Role of deep convection *Earth Space Sci.* **9** e2021EA001965
- [37] Prasad A A, Sherwood S C, Reeder M J and Lane T P 2019 Rapidly evolving cirrus clouds modulated by convectively generated gravity waves *J. Geophys. Res.: Atmos.* **124** 7327–38
- [38] Wilson R 2004 Turbulent diffusivity in the free atmosphere inferred from MST radar measurements: a review *Ann. Geophys.* **22** 3869–87
- [39] Podglajen A et al 2017 Small-Scale wind fluctuations in the tropical tropopause layer from aircraft measurements: occurrence, nature and impact on vertical mixing *J. Atmos. Sci.* **74** 3847–69
- [40] Kuebbeler M, Lohmann U and Feichter J 2012 Effects of stratospheric sulfate aerosol geo-engineering on cirrus clouds *Geophys. Res. Lett.* **39** n/a–n/a
- [41] Visionsi D, Pitari G, di Genova G, Tilmes S and Cionni I 2018 Upper tropospheric ice sensitivity to sulfate geoengineering *Atmos. Chem. Phys.* **18** 14867–87
- [42] Saint-Lu M, Bony S and Dufresne J-L 2022 Clear-sky control of anvils in response to increased CO₂ or surface warming or volcanic eruptions *npj Clim. Atmos. Sci.* **5** 78
- [43] Kroll C A, Dacie S, Azoulay A, Schmidt H and Timmreck C 2021 The impact of volcanic eruptions of different magnitude on stratospheric water vapor in the tropics *Atmos. Chem. Phys.* **21** 6565–91
- [44] Hu Z, Lamraoui F and Kuang Z 2021 Influence of upper-troposphere stratification and cloud-radiation interaction on convective overshoots in the tropical tropopause layer *J. Atmos. Sci.* **78** 2493–509
- [45] Liu Y S, Fueglistaler S and Haynes P H 2010 Advection-condensation paradigm for stratospheric water vapor *J. Geophys. Res.: Atmos.* **115** D24307
- [46] Fueglistaler S et al 2013 The relation between atmospheric humidity and temperature trends for stratospheric water *J. Geophys. Res.: Atmos.* **118** 1052–74
- [47] Smith J W, Bushell A C, Butchart N, Haynes P H and Maycock A C 2022 The effect of convective injection of ice on stratospheric water vapor in a changing climate *Geophys. Res. Lett.* **49** e2021GL097386